Hindawi Publishing Corporation
Journal of Combustion
Volume 2016, Article ID 9612856, 12 pages
http://dx.doi.org/10.1155/2016/9612856

Research Article

Experimental Study on the Influence of DPF Micropore Structure and Particle Property on Its Filtration Process

Zhongwei Meng,[1,2] Jia Fang,[1,2] Yunfei Pu,[3] Yan Yan,[1,2] Yi Wu,[1] Yongzhong Wang,[1] and Qiang Song[4]

[1] *Vehicle Measurement, Control and Safety Key Laboratory of Sichuan Province, Sichuan Collaborative Innovation Center for Automotive Key Components, School of Automobile and Transportation Engineering, Xihua University, Chengdu 610039, China*
[2] *Key Laboratory of Fluid and Power Machinery (Xihua University), Ministry of Education, Chengdu 610039, China*
[3] *Department of Automotive Engineering, Chengdu Aeronautic Polytechnic, Chengdu 610100, China*
[4] *Key Laboratory for Thermal Science and Power Engineering of Ministry of Education, Department of Thermal Engineering, Tsinghua University, Beijing 100084, China*

Correspondence should be addressed to Zhongwei Meng; mengzw@mail.xhu.edu.cn and Jia Fang; jiafang@mail.xhu.edu.cn

Received 19 September 2016; Accepted 22 November 2016

Academic Editor: Guohong Tian

Copyright © 2016 Zhongwei Meng et al. This is an open access article distributed under the Creative Commons Attribution License, which permits unrestricted use, distribution, and reproduction in any medium, provided the original work is properly cited.

A single layer filtration system was developed to investigate the filtration and regeneration performance of diesel particle filter (DPF). The particle layer thickness was directly measured online to analyze the different filtration stages. The influence of particle property on particle layer stage performance was also investigated. The results indicate that the filtration velocity can greatly affect the deep bed filtration stage, and the deposited particle layer can be compressed even in very low filtration velocity and higher filtration velocity trends to form denser particle layer. Optimizing the pore structure can effectively shorten the deep bed filtration stage and reduce the pressure drop eventually. An empirical function was proposed to relate the pore structure and the initial increment rate of pressure drop, which presented that reducing the pore size distribution range (3σ) can result in low DPF filtration pressure drop. The filtration stage could be further divided into four stages, and the value of particle layer thickness ranging within 15~20 μm has been found to be critical number for the shift from the transient stage to the cake filtration stage. Particle with large primary diameter and BET surface was beneficial to form loose particle layer.

1. Introduction

Diesel engines are widely employed for their efficient fuel consumption and low CO_2 emission, but they are also one of the widely recognized sources for particle emission, which has negative impacts on the environment and human health. Increasingly stringent legislations on vehicular emissions have triggered research interests in fuel formulations and oxygenated fuel addition [1–5], engine calibration and designs [6–9], and effective after treatment technologies [10, 11] to reduce particle and gaseous emissions. Among all the aforementioned techniques, engine calibration has limited room for emissions improvement, and the effects of oxygenated fuel addition on particle emissions are somewhat controversial [2]. Therefore, diesel particle filter (DPF) has been considered as an effective means to reduce particle emissions from diesel engines since it directly captures diesel particles to prevent their release to the atmosphere [11]. Although a DPF potentially has impressive filtration efficiencies, generally in excess of 95% and up to about 99% in mass, it requires low operating pressure drop to avoid the deterioration of the engine output power and fuel efficiency. Such a low pressure drop can reduce the DPF regeneration frequency and the fuel regeneration. Thus it is necessary to investigate the filtration mechanism and methods to minimize the pressure drop.

Typically, a three-stage filtration process, including deep bed filtration stage, transition filtration stage, and particle layer ("cake") filtration stage, was used to illustrate the particle deposition process in porous ceramic pores. The microscopic observations have been firstly conducted to show the

particle deposition process, by cutting the DPF substrate and then exposing the loaded DPF channels to obtain the surface topography above the ceramic surface. While the information of particle packing property was missed [12], the uneven particle distribution along the DPF channel was observed with the thickness being less than 100 μm, which was directly due to uneven wall flow velocity along the channel length [13]. The inhomogeneous porous particle cake was also investigated with the thickness ranged in 130 to 500 μm, and the particle cake consisted of several superposed layers corresponding to different soot generations [14]. However these offline measurements cannot quantify the particle loading and distinguish the transition of the different filtration stages. Therefore, the single DPF filtration channel system was developed to online measure the particle deposition process without cutting the DPF substrate. Based on the single channel system, evolution of the filtration process was presented by the microscopic pictures [15], and the deposited particulate volumes required to reach the transition points from deep bed to "cake" filtration were determined [16], and the packing density of particle layer can be calculated [17]. The deposited particle cake tends to present the similar packing property once the deep bed and transient stage were completed. So the deposition process in deep bed filtration stage and packing property of cake filtration stage are the two hot research points to investigate the filtration process to minimize the filtration pressure.

In the year 2007, a dense layer coated on common DPF ceramic wall was experimentally reported to control the deep bed filtration and reduce the overall filtration pressure drop [18]. This improved technology was referred to as the dual layer pore structure, in which the gas inflow side of the wall is given a filtration layer having small pores and a high porosity. It has been demonstrated to drastically improve the filtration efficiency, drastically reduce the backpressure with particle accumulation, and provide a linear relationship between soot loading and backpressure [19]. The ash loaded DPFs were found to show similar features of reducing the pressure drop [20, 21]. A numerical simulation model was applied to study the influence of pore diameter of dense layer on the particle slip and the accumulated particle inside the wall, which could obviously affect the filtration efficiency, pressure drop, and the catalytic oxidation of deposited particle in regeneration process [22]. The dual layer technology is a good way to avoid the accumulated particle inside the micropores. However, the influence of micropore structure on deep bed filtration stage has not yet been reported, which is the first motivation of our study presented in this paper.

As mentioned above, the particle packing property in cake filtration stage as another research point needs to be focused on. It is related to not only the pressure drop but also the regeneration process. While simple approaches were used to describe the soot layer, mostly assuming a constant value for soot layer density and permeability in previous research work. The values of 100 kg/m^3 and 140 kg/m^3 were mostly employed as packing density in mathematical models for the simulation of the loading and regeneration process in the DPF [23–26]. In order to validate the simulation model with the experimental results, the density values were usually selected optionally and baselessly. For example, the range of 65 to 99 kg/m^3 was applied in [27], and the values of 117 to 136 kg/m^3 were used in [28]. Thus the experimental measure of the particle layer density independently to the permeability is greatly needed. The values of 25–100 kg/m^3 were experimentally obtained by measuring the thickness and mass of particle layer deposited on single channel piece [17]. For the reason of the big experimental workload (e.g., pieces cutting and images solving), only several filtration velocities and particle loading were involved in this investigation. Furthermore, the method of cutting the single channel piece could lead to possibly damaging the deposited particle layer and obtaining large deviation on particle layer mass weighting. Therefore, the damage-free measuring of the particle layer thickness is urgently needed. The thickness can be directly measured online by the laser displacement sensor to simplify the experimental measurement, and this improvement can give a convenient for investigating the influence mechanism of the particle layer property, which is the second motivation of this study.

In the present study, a single layer channel system is developed, which can be employed to investigate both the particle filtration and regeneration process. Firstly, the filtration pressure drop of ceramic pieces under different velocity and pore structures were measured, and the deep bed filtration stage was focused on to investigate the relationship between the initial pressure drop increasing rate and the micropore structure. The dimensional analysis and experimental fitting methods were employed. Secondly, the filtration stage was analyzed based on the surface scanning electron microscope (SEM) measurement and the relationship between the thickness and pressure drop. Finally, the particle with different parameters is used to obtain the different particle cake packing densities to seek the effect of particle property on particle layer filtration process.

2. Experimental Setup and Materials

2.1. Single Layer Channel Filtration System. In order to visualize the observations of filtration process of DPF, a single layer channel filtration system is built under laboratory conditions; and the sketch map of this system is shown in Figure 1. As to the particle sources, the diesel engines exhaust soot, carbon black particle, and fuel (e.g., Propane) combustion generated soot are considered and flow into the single layer channel part separately through bypass valve control. When the diesel engine or the fuel burner are acted as soot generator, the inlet pipe and single layer channel part are heated and thermal insulated at the constant temperature 200°C. It is aimed at avoiding the water and volatile organic compounds (VOC) of the exhausted gas condensed in the single layer channel part. The condensed water and VOC can destroy the deposited particle layer resulting in a failure to obtain the expected experimental data correctly. Besides the heating, the thermal insulation can reduce the particle thermophoresis deposition in the sample pipe, so the particle concentration can be preserved uniformly, except for the fluctuation of the operating

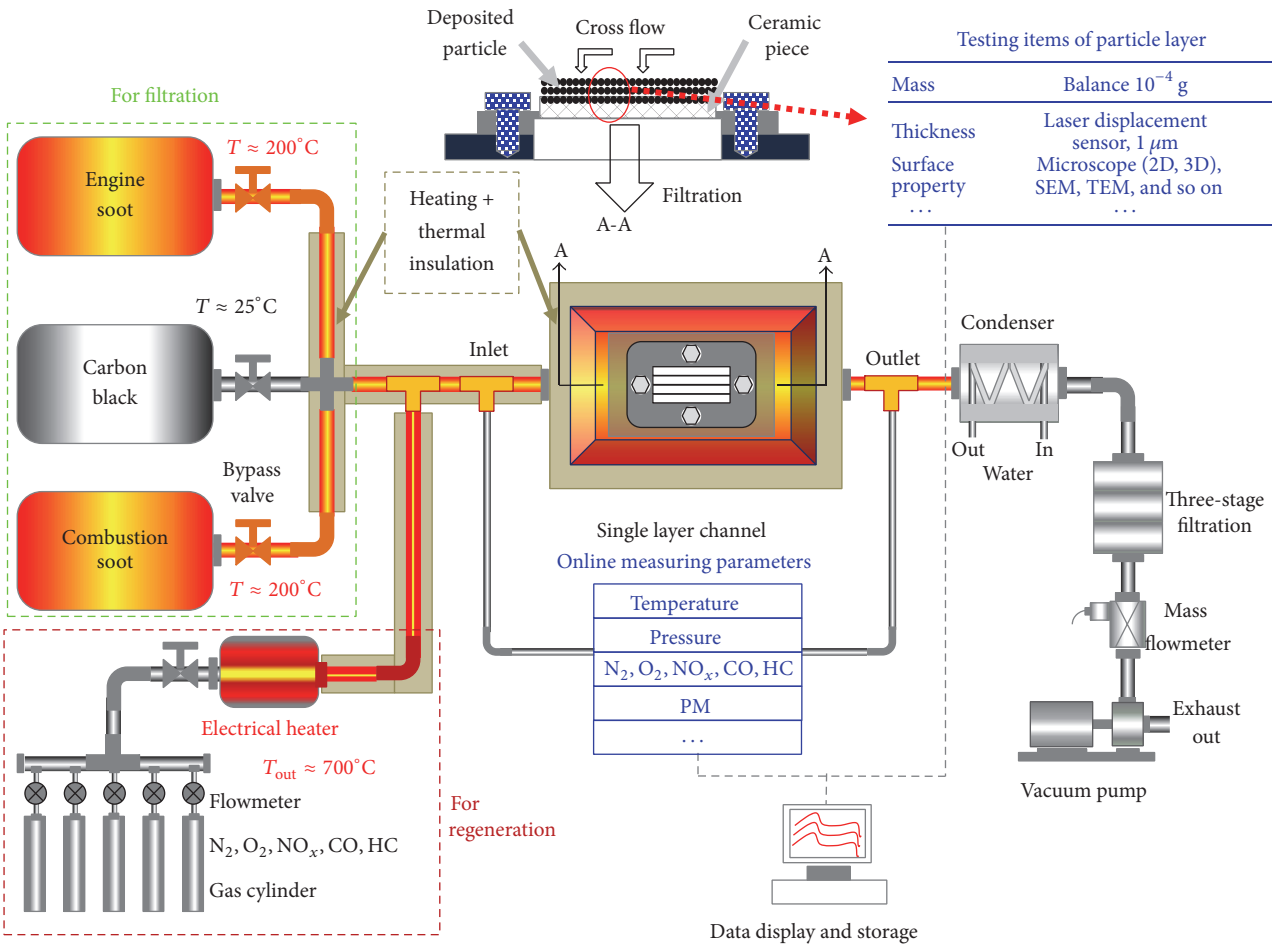

Figure 1: The schematic diagram of single layer channel filtration system.

condition of the particle source. When applying the carbon black particle as the substituted or artificial diesel engine soot, the filtration process is conducted at the room temperature of about 25°C. The dried commercial carbon black is prepared before the experiment and then homogenously dispersed by an aerosol generator *(Palas RBG1000)* to simulate the diesel engine exhaust soot.

As to the single layer channel part, a single layer of ceramic piece (30×60 mm^2) cutting from a whole wall flow ceramic DPF filter is mounted in the middle of this part, which is attached to the stainless steel (SS) plate using high temperature cement *(OMEGABOND® OB-400)* and fastened the SS plate by 4 bolts with M8 mm. The real pictures of the ceramic piece and its attached SS plate before and after the soot deposition are shown in Figure 2. The deposited particle mass can be measured by weighting the ceramic piece together with the SS plate before and after the particle deposition using an electronic balance with the accuracy of 10^{-4} g. The surface topography of particle layer on ceramic piece can also be measured offline by microscope or SEM/TEM (transmission electron microscope) method, which can directly show the microscopic and detail variation information of the particle deposition process. The particle deposition process on the ceramic

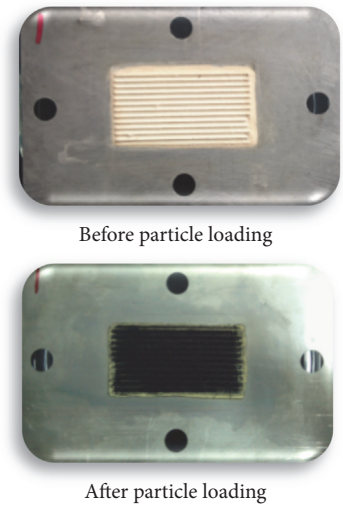

Figure 2: The ceramic pieces.

piece surface can also be directly observed through the visualization window (Quartz glass) in the upright cover just above the ceramic piece. The picture of the visualization window

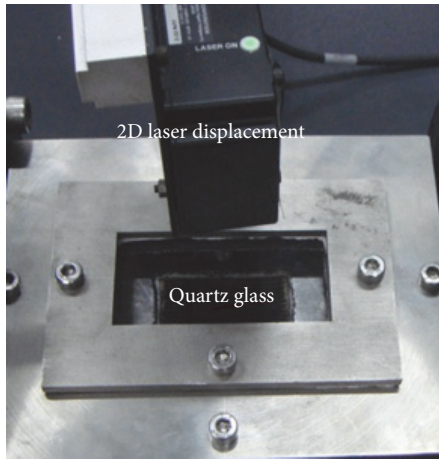

Figure 3: The visualization window.

is shown in Figure 3. A 2D laser displacement sensor *(LJ-G080, Keyence)* is applied to online measure the thickness of particle layer through the visualization window. The LJ-G080 sensor has 650 testing points with the accuracy of 1 μm, which is capable of measuring the evolution of particle layer deposition during the filtration process.

Besides, the other online measuring parameters at the inlet and outlet of the single layer channel are temperature, pressure drop, exhaust gas concentration, and particulate matter (PM) mass and number distribution. The temperature is measured by K-type thermocouples, and pressure drop is measured by U-type manometer or high accuracy pressure transducers *(OMEGA's PX409-005CG5V)* with the measure ranges less than ±35 kPa. The gas concentrations are measured by *AVL DICOM4000* or *MRU NOVA PLUS* gas analyzer. The PM mass and number distributions are measured by the *CAMBUSTION DMS500* fast particle analyzer.

As to the single layer channel configuration, the channel height is selected for 15 mm, which is larger than the 1.16 mm for 300 CPSI DPF or 2.16 mm for 100 CPSI DPF. The reason of this design is to facilitate the mechanical machining of the SS frame and convenient for installing and removing the single layer ceramic piece. The researched particle diameter is normally smaller than 300 nm, so the particle in aerosol has good tracking capability with the cross flow. Although the cross flow pattern of single layer channel is different from that of honeycomb channel of DPF filter, the particle deposition processes on the ceramic surface of these two flow patterns have good consistency with each other. In this system, the particle deposition process normal to the ceramic surface is just focused on, while the particle migration potentially driven by the main flow direction parallel to ceramic surface is ignored.

As to the single layer channel operating pressure, because the particle sources are connected to the single layer channel through the bypass pipes, and the redundant exhaust is directly discharged into the atmosphere, so the inlet pressure of the single layer channel is nearly the atmospheric pressure. Actually the particle is absorbed into the single layer channel for filtration driven by a vacuum pump. The operating pressure of the single layer channel system is actually different from the real DPF system. The range of about 90–100 kPa is normally for the former one, while the range of about 100–115 kPa is normally for the later one. The variation of the operating pressure can cause the variation of operating temperature and particle concentration, while this deviation can be estimated and limited into a certain degree. The filtration velocity (flow rate) is controlled by a thermal wire type mass flowmeter, shown in Figure 1. The vertical filtration velocity in this system is set to 0.02–0.15 m/s, which is in accordance with the wall flow filtration velocity of the real honeycomb DPF filter. Before the exhaust from the single layer channel flow into the mass flowmeter, the exhaust is cooled by a condenser, and then the condensed water and VOC fraction and the penetrated particle from the single layer channel are absorbed and filtered by a three-stage filtration system, to protect the mass flowmeter and ensure the measure accuracy.

On the other side, after the ceramic piece is loaded with particle through the filtration process, the combustion of the loaded particle layer can also be visually observed by this single layer system. The regeneration of deposited particle layer can be conducted by elevating the inlet exhaust temperature lager than 550°C to oxidize it, using an electrical heater *(MHI MTA925-02)* with maximum outlet temperature being about 700°C. The gas concentration and mass flowrate for the regeneration are controlled by the gas cylinder group and their flowmeters for each of them. Because the reason of this paper is not focused on the regeneration process, the detailed information of the regeneration function of this single layer channel system is just illustrated simply so far.

2.2. Particle Sources. In this study, a one-cylinder diesel generator CF5000LN (0.406 L, wind cooled, 9 kW/3600 RPM) and a four-cylinder diesel engine DK4A (2.5 L, common rail, turbo charged, 75 kW/3600 RPM) are used to produce diesel soot as the soot generator. The CF5000LN generator is operated at 70% engine full load with the exhaust temperature about 350°C, while the DK4A engine is operated at the load of 57 Nm/2250 RPM with the exhaust temperature about 290°C.

Besides, four-type Degussa carbon blacks (Printex-U, SB 4A, CB FW200, SB250) are also used as substituted soot to investigate the particle deposition process. The particle properties of these carbon blacks together with the DK4A engine soot are shown in Table 1, and the microscopic TEM (TECNAI G2 F20) picture of these particles is also shown in Figure 4. The primary diameter data of different particles are their statistical mean values among more than 20 particles selected from the TEM pictures using image processing software. The values of Brunauer-Emmett-Teller (BET) surface, VOC, and ash contents of carbon black are provided by manufacturers. The VOC content of DK4A soot is measured by vacuum dry method, while the BET surface and ash content of DK4A soot are not presented in this paper. The DK4A soot is collected directly from the engine rail pipe using the multiplayer stainless steel mesh filter and the sample mass obtained about 40 mg per hour under a steady state engine condition.

The Special Black (SB) 250 particles have the largest primary diameter of 51 nm, while the lowest BET surface (40 m^2/g) is shown. The Carbon Black (CB) FW 200 particles

Table 1: The parameters of different particles.

Particles	Primary diameter (nm)	BET (m^2/g)	VOC (%)	Ash (%)
DK4A soot	24	NA	4.1	NA
Printex-U	34	92	5.0	0.02
SB 4A	44	180	14.5	0.02
CB FW200	20	550	20.0	0.02
SB 250	51	40	3.5	0.4

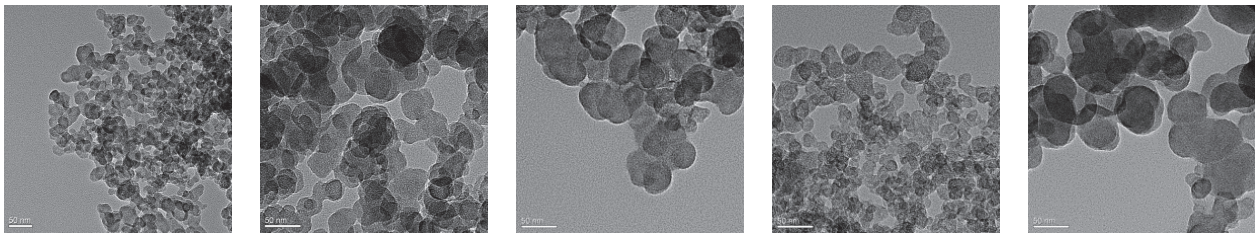

(a) DK4A soot (b) Printex-U (c) SB 4A (d) FW200 (e) SB 250

Figure 4: The TEM pictures of different particles.

have the smallest primary diameter of 20 nm, while the highest BET surface (550 m^2/g) is shown. The VOC content of the DK4A soot is about only 4.1%, and although the VOC contents of SB 4A and CB FW200 particles are relatively large as 14.5% and 20.0% separately, the carbon black particles are operated in room temperature of about 25°C; thus the influence of VOC on particle filtration process is ignored in this paper. Besides, the ash contents of carbon black particles are smaller than 0.4% at the most, which is believed to be larger than the ash content of DK4A soot; thus the influence of ash content on particle filtration process is also ignored in this study.

2.3. Micropore Structure of Experimental Ceramic Pieces. There are seven types of ceramic pieces used in this study, which are randomly cut from filters from different four DPF suppliers (one is American company, and the other three ones are domestic manufacturers). The micropore structures of these ceramic pieces are shown in Table 2, which are measured by a mercury porosimeter *(Micromeritics, AutoPore IV 9510)*. The porosities of the tested pieces ranged from 13.88% to 51.34%, while the average pore diameters ranged from 5.59 μm to 12.16 μm.

Table 2 also shows the value of three standard deviations (3σ), which is obtained from the Gaussian fitting the pore size distribution curves of different tested ceramic pieces. The Gaussian fitting curves of three ceramic pieces, for example, are shown in Figure 5, and the values of the 3σ ranged from 2.91 to 12.43 μm, which are capable of representing the micropore size distribution of ceramic pieces.

The #1 ceramic pieces were prepared to study the influence of filtration velocity (0.02–0.04 m/s) on the filtration process, while the #2 to #4 pieces were used for 0.02 m/s filtration velocity condition, and the #5 to #7 pieces were used for 0.04 m/s condition to study the influence of pore structure on the filtration process in Section 3.1 in this paper. Besides,

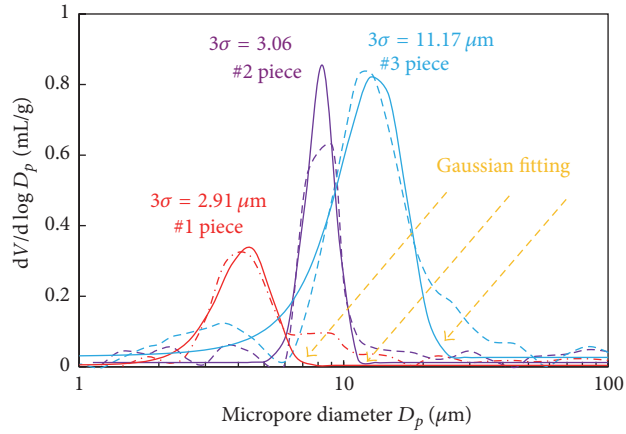

Figure 5: Gaussian fitting of tested ceramic pieces.

the #1 ceramic pieces are also used to conduct the research work of Sections 3.3 to 3.5.

3. Experimental Results and Discussion

3.1. Filter Pressure Drop. The pressure drop of #1 ceramic pieces is measured for testing with different filtration velocities, and the diesel generator CF5000LN is used as particle source, and the operating temperature is kept at 200°C for steady state filtration test. With the increase in particle loading time, the pressure drop increases along with the deposited particle to present the typical three-stage filtration process, which is shown in Figure 6. With the increase in filtration velocity, the deposited particle into the micropores of ceramic piece in unit time is increased, which led to rapidly completing the deep bed and transient filtration stage under high filtration velocity condition. The initial increment rates are obtained by fitting the first 120 s data of pressure drop

Table 2: Filter pore structures.

Ceramic pieces	Porosity ε_w/%	Average pore diameter D_p/μm	Three standard deviations (3σ)/μm
#1	15.70	5.59	2.91
#2	26.57	7.08	3.06
#3	51.34	12.16	11.17
#4	19.82	6.00	8.80
#5	47.06	11.02	12.43
#6	13.88	6.40	2.88
#7	18.29	6.48	3.18

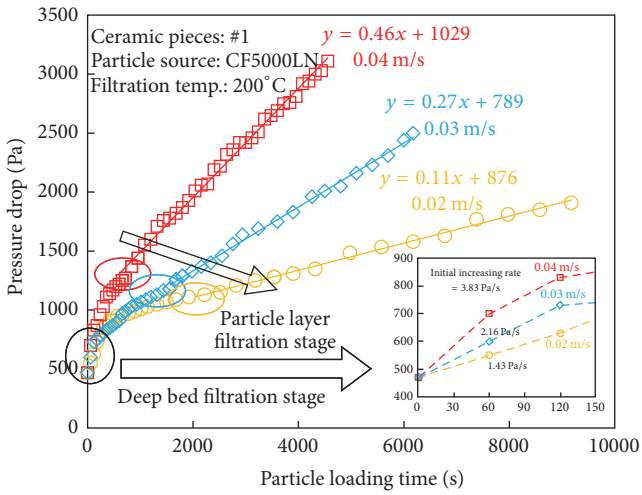

Figure 6: Pressure drop for different filtration velocities (in order to conveniently compare the increment rates of the pressure drop for different filtration velocities, the initial pressure drops are set to the same value of 470 Pa which is measured for the 0.02 m/s filtration velocity).

curve, with the values being 1.43 Pa/s for 0.02 m/s filtration velocity, 2.16 Pa/s for 0.03 m/s, and 3.83 Pa/s for 0.04 m/s, respectively. It is attributed to the increasing deposited particle mass in unit time and filtration velocity, which is defined by Darcy's formula. The micropores are gradually blocked by deposited particle causing the ceramic piece permeability to gradually decrease. For the reason of the micropores being not blocked homogenously with loading time, the increment rate of pressure drop curve gradually decreased with loading time; thus the initial increment rates of first 120 s are used to evaluate the deep bed filtration process. The particle tends to more easily penetrate the ceramic piece in higher filtration velocity, so the deposited particle mass dividing the filtration velocity in higher filtration velocity condition is smaller than that of lower filtration velocity. Therefore, the initial increment rate does not increase quadratically with filtration velocity. For example, comparing with the two operating conditions of the 0.02 and 0.04 m/s, the value of 3.83/1.43 = 2.68 is clearly smaller than the value $(0.04/0.02)^2 = 4$ and the relative deviation is about 33%.

The starting times of particle layer filtration also obviously decrease with the increase in filtration velocity, shown in Figure 6. The particle layer filtration stags appear after about 1900 s for 0.02 m/s filtration velocity, 1300 s for 0.03 m/s, and 600 s for 0.04 m/s, which are approximately evaluated from the pressure drop curves. The pressure drop increment rates during the particle layer filtration stage are fit and shown with straight line with the increment rate values being 0.11 Pa/s for 0.02 m/s, 0.27 Pa/s for 0.03 m/s, and 0.46 Pa/s for 0.04 m/s filtration velocity, respectively. After the particle layer is formed, the particle filtration efficiency is kept constantly up to about 99% generally. So the value of deposited particle mass in unit time divided by the filtration velocity in particle layer filtration stage is kept nearly constantly for different filtration velocity. Based on this reason, the increment rate of pressure drop increases approximately quadratically with the increase in filtration velocity. For example, comparing with the two operating conditions of the 0.02 and 0.04 m/s, the value of 0.46/0.11 = 4.18 is near the value of $(0.04/0.02)^2 = 4$; the relative deviation is only about 4.5%, which is obviously smaller than 33% in deep bed filtration stage. However, the particle layer would tend to become denser in high filtration velocity, which should be taken into account under the condition of higher filtration velocity.

Although the different filtration velocity has significant effect on the deep bed filtration, once the particle layer is formed, the particle layer filtration process would present similar changing trends under different filtration velocities. This result suggests that decreasing the pressure drop of deep bed and transient filtration stage may be the only way to decrease the DPF pressure drop under the steady state filtration condition. This is also the original cause of dual layer filtration technology illustrated in the Introduction part of this paper. Therefore, different pore structure ceramic pieces are used to investigate the influence of micropore structure on filtration process, which is targeted to find the relationship between the pore structure and deep bed filtration process and ultimately obtain the optimization region or method to decrease the DPF pressure drop.

The measured pressure drop curves for different pore structure pieces with the 0.02 m/s and 0.04 m/s filtration velocities are shown in Figure 7. The slopes of the pressure drop curves during the particle layer filtration stage have little difference for the different pore structures for the same

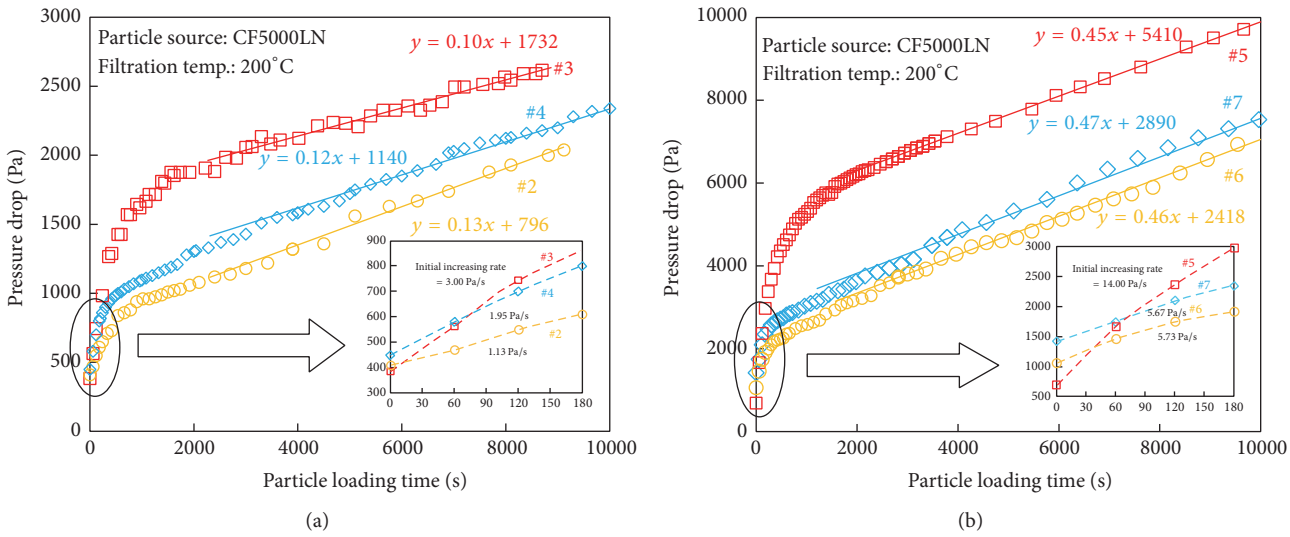

Figure 7: Pressure drop of different pore structure pieces: (a) filtration velocity = 0.02 m/s and (b) 0.04 m/s.

filtration velocity. The relative deviations are about 16% and 4% for two filtration velocities. The reason is that the flow through the deposited particle layer mainly depends on the soot properties and the filtration velocities, and the particle layer characteristics are no longer subjected to the structure of the ceramic micropores below it.

The pore structure has obvious effects on the pressure drop during the deep bed filtration and transition filtration stages. The filter with higher initial pressure drop increment rate and longer transition filtration stage has higher pressure drops during particle layer filtration stages. Thus, proper ceramic filter will reduce the pressure drop and delay the regeneration period which will reduce the fuel penalty during the filter regeneration process. If the pressure drop limit for filter regeneration is selected as 6000 Pa, for example, filter #5 would need to be regenerated after about 1500 s, while filter #6 would need about 8000 s under the same operating condition, shown in Figure 7(b). Thus optimizing the pore structure is effective to reduce the DPF pressure drop. The initial increment rates are also fitted and marked in Figure 7 using the first 120 s data of pressure drop curves. Higher initial increment rate tends to cause higher DPF pressure drop. Therefore, investigation on the relationship between the pore structure and initial increment rate is quite useful to select and optimize the DPF pore structure.

3.2. The Relationship between the Pore Structure and Initial Increment Rate of Pressure Drop. There are 9 values of initial increment rate $(d\Delta P/dt)_{initial}$ marked in Figures 6 and 7 for different pore structures and filtration velocities. However the values of $(d\Delta P/dt)_{initial}$ cannot be simply correlated with only one parameter of the velocity u, or the porosity ε_w, or the average pore diameter D_p and or the pore size distribution range 3σ, shown in Table 1. Thus a multiparameter correlation method is applied to empirically fit the data. Firstly, the Buckingham π theorem was used for a dimensional analysis

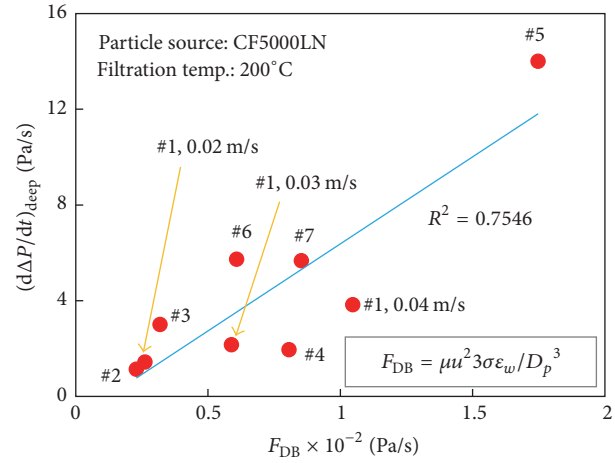

Figure 8: The relationship between $(d\Delta P/dt)_{initial}$ and F_{DB}.

to correlate $(d\Delta P/dt)_{initial}$ with u, ε_w, D_p, 3σ, and the exhaust dynamic viscosity μ as follows:

$$\left(\frac{d\Delta P}{dt}\right)_{deep} \propto \frac{\mu u^2 3\sigma \varepsilon_w}{D_p^3} = F_{DB}. \quad (1)$$

From (1), the values of $(d\Delta P/dt)_{initial}$ are directly proportional to the viscosity μ, u^2, 3σ, and ε_w and inversely proportional to D_p^3. The values of the parameter F_{DB} defined by (1) are calculated using the above parameters, and the relationship between $(d\Delta P/dt)_{initial}$ and F_{DB} is presented in Figure 8. $(d\Delta P/dt)_{initial}$ is found to generally increase with F_{DB}, while the points are dispersed along the linear fitting curve with the coefficient of determination $R^2 = 0.7546$. Equation (1) is just a dimensional analysis for the parameter of $(d\Delta P/dt)_{initial}$. The detailed physical process is ignored in this analysis, and the large deviation is obtained by directly using this correlation.

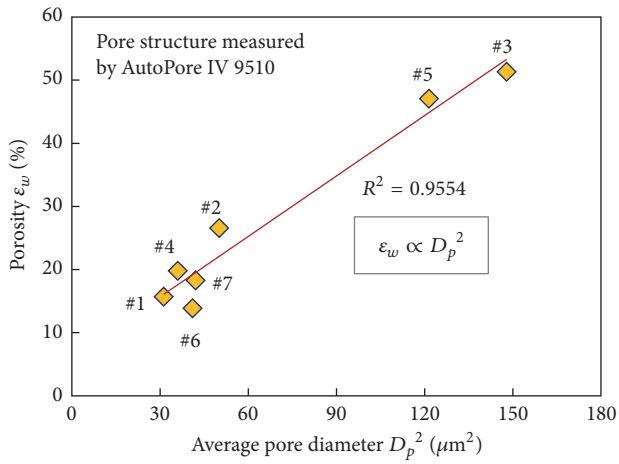

FIGURE 9: The relationship between the porosity ε_w and the diameter D_p.

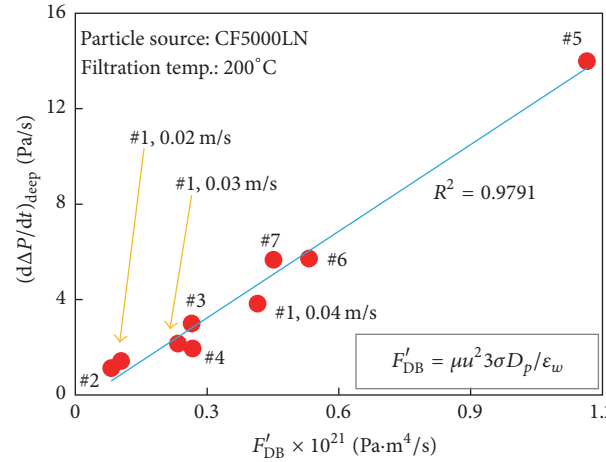

FIGURE 10: The relationship between $(d\Delta P/dt)_{initial}$ and F'_{DB} after revising parameter F_{DB}.

The bad linear fitting can be attributed to the definitions of filtration velocity and porosity in (1). Firstly, as it has been mentioned above in Section 3.1, the initial increment rate does not increase quadratically with filtration velocity; thus the quadratic variation leads to large deviation from the linear fitting, which needs to be corrected. Secondly, larger porosity of ceramic piece would lead to lower filtration velocity and bigger particle deposition surface in micropores, so $(d\Delta P/dt)_{initial}$ would be inversely proportional to the porosity theoretically, which is contradicted to (1) variation trend. In practical condition, the porosity ε_w is actually varied together with the diameter D_p. A particular experimental relationship between them is generated during the material manufacturing process without theoretical basis. A corresponding quadratic relationship of the porosity ε_w with the diameter D_p is clearly observed in Figure 9 with the linear fitting deviation $R^2 = 0.9554$. This quadratic correlation is an experimental curve fitting of just 7 data points provided by four DPF manufactures. The data sample numbers are very limited, but we believe this relationship has certain representation to a certain degree.

Based on the special relationship between the porosity ε_w and the diameter $D_p(\varepsilon_w \propto D_p^2)$, the revised parameter F_{DB} is defined in (2) as follows:

$$\left(\frac{d\Delta P}{dt}\right)_{deep} \propto \frac{\mu u^2 3\sigma D_p}{\varepsilon_w} = F'_{DB}. \quad (2)$$

In (2), the values of $(d\Delta P/dt)_{initial}$ are proportional to D_p and inversely proportional to ε_w. The relationship between $(d\Delta P/dt)_{initial}$ and the revised parameter F'_{DB} defined by (2) is shown in Figure 10. The linear fitting degree is effectively improved as $R^2 = 0.9791$.

This relationship among various parameters in (2) is quite reasonable for DPF application. Firstly, increasing D_p without changing ε_w means to reduce the micropore numbers, which would enhance the plugging degree in micropores and lead to increase in the initial increment rate of pressure drop in deep bed filtration stage. Secondly, if the porosity ε_w is increased while D_p is kept constant, the micropore number would be increased to provide larger filtration surface, which would obviously reduce the value of $(d\Delta P/dt)_{initial}$. Besides, as to the dual layer filtration technology, the upper layer has very smaller pores and very thinner thickness compared with the lower layer, which leads to significantly decreasing the average micropore size D_p and slightly decreasing the porosity ε_w. Therefore, $(d\Delta P/dt)_{initial}$ can be decreased to obtain low DPF pressure drop using the dual layer technology compared with the common or regular DPF design.

Particularly, both (1) and (2) present the same variation relation between $(d\Delta P/dt)_{initial}$ and the pore size distribution range (3σ). Reducing 3σ would reduce the value of the $(d\Delta P/dt)_{initial}$ and eventually lead to low final DPF pressure drop. Large value of 3σ means large number of the smaller micropores appearing in porous wall. Smaller micropores would act as the throat of the microflow channel in porous wall, which will result in high pressure drop during deep bed filtration process. Therefore, reducing the pore size distribution range (3σ) can improve the homogenization of the microfiltration flow in porous wall, which gives an effective method to optimize the pore structure and reduce the DPF filtration pressure drop.

3.3. Microscopic Measurement of Particle Deposition Process. In order to conveniently observe the particle deposition process, the SEM method was applied and the results are shown in Figure 11. Four stages are observed in particle deposition process, which is in accordance with [15]. The particle deposition process can be divided as follows: Stage I, deep bed filtration stage: particles mainly deposit inside the micropores and gradually block it, while particles rarely deposit on skeletal position between adjacent micropores, shown in Figure 11(a); Stage II, particle tree growth stage: particles continually deposit into the micropores to form a particle trees (about 20~30 μm) just above the micropores, just like several "particle bread" growing from the micropores position with the heights above the ceramic surface, shown in Figure 11(b);

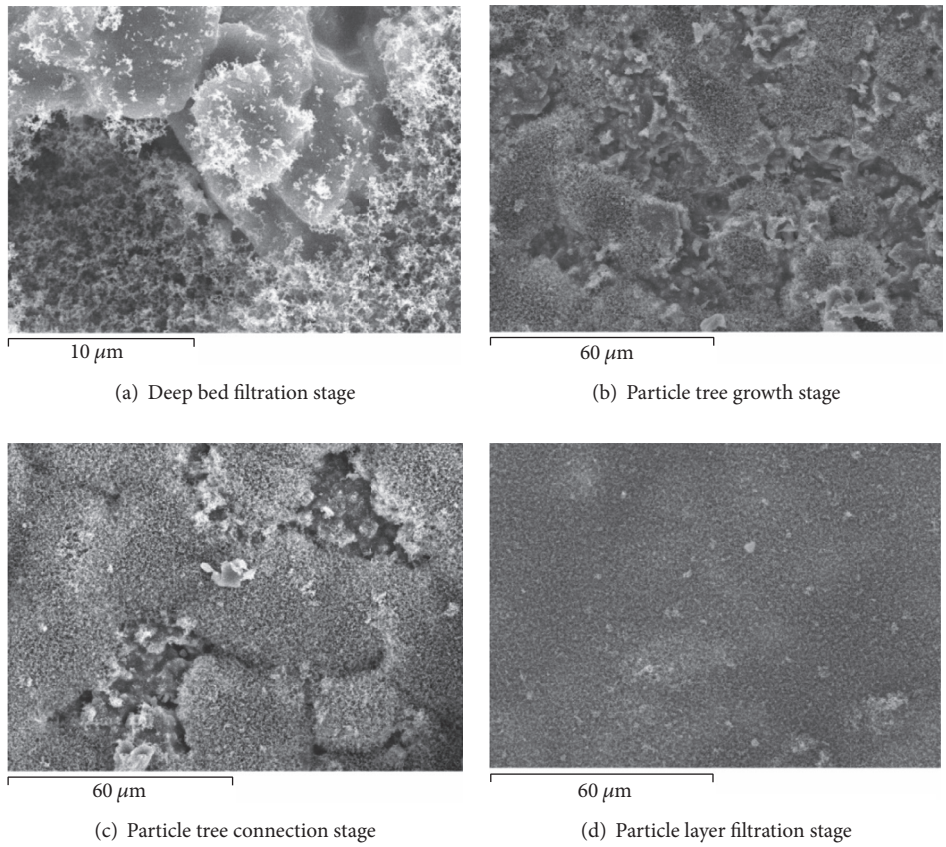

(a) Deep bed filtration stage (b) Particle tree growth stage

(c) Particle tree connection stage (d) Particle layer filtration stage

Figure 11: The SEM images of the surface of ceramic piece in different filtration stage (particle source: CF5000LN; filtration temp. = 200°C; filtration velocity = 0.02 m/s; #1 ceramic pieces).

Stage III, particle tree connection stage: particle trees gradually become "fat" and grow up (about 40~50 μm); inlet particles gradually deposit on the particle trees and make the particle trees connect with each other, shown in Figure 11(c); Stage IV, particle layer filtration stage: after the particle trees connect each other to cover the whole ceramic surface, the inlet particle deposit on the flat surface of the connected particle trees to form the particle layer, shown in Figure 11(d). Generally, as to the typical three-stage filtration process, the transient filtration stage could be further divided into the particle tress growth and connection stages.

Different pore structure presents different deep bed filtrations, particle tree growth, and connection stages. Once the particle layer is formed, the deposited particle layer property is nearly independent of the micropore structure just below it. Therefore, except the investigation on the influence of micropore structure on deep bed filtration stage, the effect of particle property on deposited particle layer characterization is also another hot research topic and needs to be further investigated. The SEM microscopic measurement has the limitation just for qualitatively analyzing, not for quantitatively evaluating. Thus the 2D laser displacement measurement is applied to online measure the thickness of the particle layer to understand the particle deposition process.

3.4. The Thickness of Deposited Particle Layer. The particle layer thickness is online measured and correlated with pressure drop under 0.02 m/s filtration velocity condition, which is shown in Figure 12. Two different particles are employed; one is DK4A diesel engine soot, and the other is Printex-U carbon black. The measured particle layer thickness is less than 50 μm. As to the DK4A soot, the loading time to obtain the particle layer thickness of 37 μm is about 13740 s, while the time is 1110 s to get about 50 μm particle layer thickness using the high concentration particle generator (Printex-U), compared with the low particle concentration of engine exhaust gas.

With the increase in the particle layer thickness, the pressure drop presented the similar variation trend with the relationship between pressure drop and loading time, shown in Figures 6–8. The pressure drop cures first increase rapidly and then decelerate the increment rate in the cake filtration stage. The pressure drop increases sharply when the particle layer thickness is less than about 3 μm, because the particles are mainly deposited into the micropores of ceramic piece, rather than deposited on the ceramic piece surface. So the pressure drop increases sharply, but the particle layer thickness is close to the initial status (near zero). This process is referred to as the deep bed filtration stage. After that, the particles start

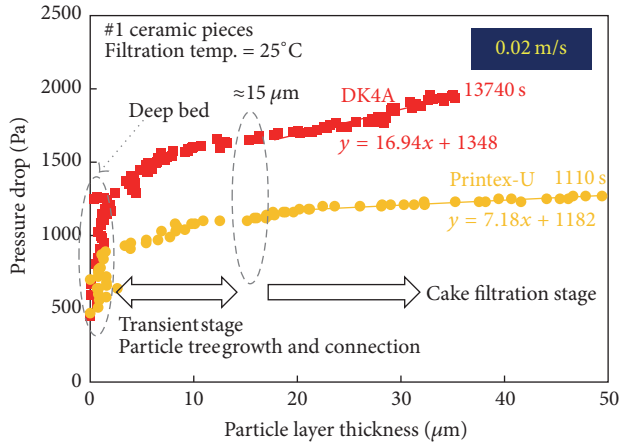

FIGURE 12: The pressure drop of ceramic pieces with the particle layer thickness.

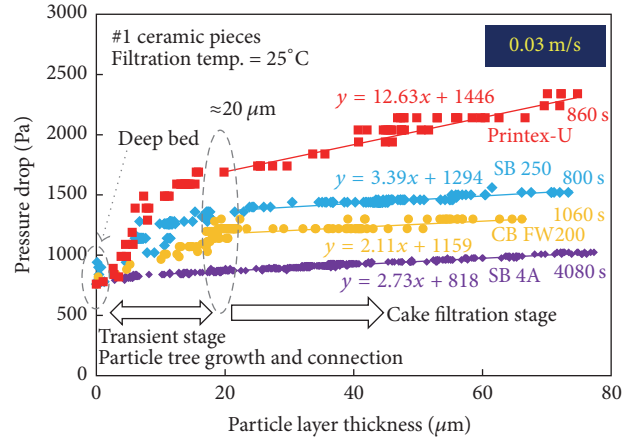

FIGURE 13: The pressure drop of different carbon black particles.

to deposit on the ceramic surface to form particle trees and then connect each other to form the flat particle layer. During the particle tree growth and connection process, the pressure drop increases nonlinearly with the particle layer thickness. The curves are similar to those of pressure drop versus the loading time. When the particle layer thickness is larger than a critical value (about 15 μm, in Figure 12), the pressure drop changes near linearly with the thickness. In this cake filtration stage, the particle layer presented to form homogeneous depositing particle layer, which leads to linear relationship between pressure drop and thickness.

Besides, the pressure drop increment rate of DK4A soot is more than two times larger than that of Printex-U particle during the particle layer filtration stage, shown in Figure 12. Although the curve of DK4A soot is measured at 200°C rather than 25°C for the Printex-U particle, the conclusion of the DK4A soot layer being denser than the Printex-U particle layer can be obtained by applying the Darcy Equation ($\Delta P = \mu \cdot u \cdot \delta_p / K_p$) to get the increment rate of $(\mathrm{d}\Delta P/\mathrm{d}\delta_p)_{\mathrm{cake}} = \mu \cdot u / K_p$ (where δ_p means the particle layer thickness and K_p means the particle layer permeability). Previous studies have shown that the Printex-U particle can be served as the artificial diesel engine soot, while the particle property and particle packing property have certain difference to be noticed in the following study. Then influence of particle property on pressure drop of particle layer is studied, which is target to find a possible way to reduce the particle layer pressure drop by varying the particle property.

The pressure drop of different carbon black particles is shown in Figure 13. The filtration is selected as 0.03 m/s rather than 0.02 m/s, which is aimed at shortening the deep bed filtration stage to get different filtration process for comparison. The process of that pressure drop increases sharply while the thickness close to zero was clearly limited, for the deposited mass in unit time increasing to rapidly block the micropores to form particle tree. The shift value of particle layer thickness to start the cake filtration was delayed to about 20 μm rather than 15 μm. The possible reason may be that larger velocity tends to form higher particle tree in the typical transient stage. The Printex-U particle presents the highest pressure drop value and increment rate compared with the other three carbon black particles, while the SB 4A particle shows the lowest pressure drop value and relative smaller increment rate in cake filtration stage. For the reason of only four particle samples, the clear correlation principle between the particle property and pressure drop cannot be curtly proposed, while the particle with large primary diameter and BET surface tend to present low pressure drop. For example, although the SB 250 particle has the largest diameter (51 nm), it also has the lowest BET surface (40 m^2/g), so it presents higher pressure drop and increment rate than CB FW200 and SB 4A particle. The CB FW200 particle has the largest BET surface (550 m^2/g), while it has smaller primary diameter (20 nm) compared with the SB 4A particle (44 nm, 180 m^2/g). So the CB FW200 particle shows higher pressure drop than SB 4A particle, while it has smaller increment rate (2.11 Pa/μm) than that of SB 4A particle (2.73 Pa/μm). Therefore, large primary diameter and BET surface could be beneficial to form loose particle layer to decrease the pressure drop and increment rate.

3.5. The Bulk Density of Deposited Particle Layer. Based on the measured particle layer thickness, its packing density can be obtained by weighting the deposited mass on the ceramic surface before and after particle loading, the results are shown in Figure 14. In order to investigate the compressed characterization of deposited particle layer, the filtration velocities were selected up to 0.15 m/s, which is larger than the general limit value of 0.05 m/s for usual operating condition of DPF. With the increase in the filtration velocity, the packing density increases rapidly in the low filtration velocity and then starts to slow down the increment rate when the velocity is larger than about 0.1 m/s. This result showed that the particle layer could be compressed more obviously in low filtration velocity; high filtration velocity leads to high packing density. The values packing densities range within 70~92 $\mathrm{kg/m}^3$ for Printex-U, 75~105 $\mathrm{kg/m}^3$ for DK4A, 78~118 $\mathrm{kg/m}^3$ for CB

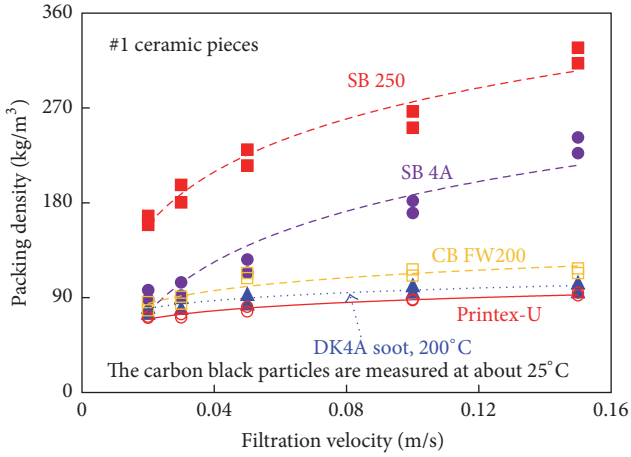

FIGURE 14: The packing density of the different particles.

FW200, 88~242 kg/m^3 for SB 4A, and 160~327 kg/m^3 for SB 250, respectively.

The packing density seems to be related more to the primary diameter than to the BET surface of the particles. The SB 250 particle presents the largest packing density, because it has the largest primary diameter; even its BET surface is the smallest one. Although the CB FW200 has the highest BET surface, it presents a relative smaller packing density compared with SB 250 and SB 4A particles, because it has the lowest primary diameter among them. As to the packing density, the Printex-U particle shows nearly the similar variation trend with the DK4A diesel engine soot.

4. Conclusions

Based on the experimental study presented in this paper, the following conclusions can be drawn.

(1) The single layer channel system is proved to be capable of investigating the particle deposition process on porous ceramic surface. Except for the pressure drop and the microscopic observation, the particle layer thickness can be measured online directly for analyzing, which gives a good tool for visualizing the DPF filtration and regeneration research.

(2) Increasing the filtration velocity can obviously decrease the deep bed filtration period, while once the particle layer is formed, the particle layer filtration process would present similar changing trends under different filtration velocities.

(3) Increasing the filtration velocity, particle layer is obviously compressed to result in the packing density increases rapidly in the low filtration velocity and then starts to slow down the increment rate when the velocity is larger than about 0.1 m/s.

(4) The pore structure can greatly affect the deep bed filtration to show different pressure drops. The piece with higher initial increasing pressure drop rates and longer transition filtration stages shows higher pressure drop during particle layer filtration stage.

(5) An experimental fitting equation for correlating the pore structure and initial increment rate of deep bed filtration has been proposed. Reducing the pore size distribution range (3σ) can improve the homogenization of the microfiltration flow in porous wall, and it can effectively result in low DPF filtration pressure drop.

(6) The filtration process can be further divided into four progressive stages: deep bed, particle tree growth, particle tree connection, and particle layer filtration stages. The typical transient filtration stage could be further divided into the particle tree growth and connection stages, which are observed by SEM method and online thickness measurement. Besides, the thickness ranging within 15~20 μm has been found for the shift value of the transient stage to the cake filtration stage.

(7) During the particle layer filtration stage, particle with large primary diameter and BET surface is beneficial to form loose particle layer to decrease the pressure drop and increment rate, while the packing density seems to be related more to the primary diameter than to the BET surface.

Competing Interests

The authors declare that there is no conflict of interests regarding the publication of this paper.

Acknowledgments

This work has been supported by (1) The National Natural Science Foundation of China (51676167); (2) the Chunhui Plan of the Ministry of Education of China (Z2014058); (3) the Industry Cluster project for Electronic Engine Control Systems and After Treatment Systems of Chengdu, China (2013-265); (4) Research Project of Key Laboratory of Fluid and Power Machinery (Xihua University), Ministry of Education (SZJJ2016-005); (5) Science & Technology Department of Sichuan Province (2015TD0021, 2017TD0026); and (6) the Innovation Foundation of Xihua University (YCJJ2015040, YCJJ2016087) [1].

References

[1] A. Ben Amara, R. Dauphin, H. Babiker et al., "Revisiting diesel fuel formulation from Petroleum light and middle refinery streams based on optimized engine behavior," *Fuel*, vol. 174, pp. 63–75, 2016.

[2] L. Chen, R. Stone, and D. Richardson, "A study of mixture preparation and PM emissions using a direct injection engine fuelled with stoichiometric gasoline/ethanol blends," *Fuel*, vol. 96, pp. 120–130, 2012.

[3] F. Millo, D. S. Vezza, T. Vlachos et al., "Particle number and size emissions from a small displacement automotive diesel engine: bioderived vs conventional fossil fuels," *Industrial and*

Engineering Chemistry Research, vol. 51, no. 22, pp. 7565–7572, 2012.

[4] L. Chen, Z. Zhang, W. Gong, and Z. Liang, "Quantifying the effects of fuel compositions on GDI-derived particle emissions using the optimal mixture design of experiments," *Fuel*, vol. 154, pp. 252–260, 2015.

[5] E. G. Giakoumis, C. D. Rakopoulos, A. M. Dimaratos, and D. C. Rakopoulos, "Exhaust emissions of diesel engines operating under transient conditions with biodiesel fuel blends," *Progress in Energy and Combustion Science*, vol. 38, no. 5, pp. 691–715, 2012.

[6] H. Lee and Y. Jeong, "The effect of dynamic operating conditions on nano-particle emissions from a light-duty diesel engine applicable to prime and auxiliary machines on marine vessels," *International Journal of Naval Architecture and Ocean Engineering*, vol. 4, no. 4, pp. 403–411, 2012.

[7] L. Chen, R. Stone, and D. Richardson, "Effect of the valve timing and the coolant temperature on particulate emissions from a gasoline direct-injection engine fuelled with gasoline and with a gasoline-ethanol blend," *Proceedings of the Institution of Mechanical Engineers, Part D:*, vol. 226, no. 10, pp. 1419–1430, 2012.

[8] P.-Q. Tan, S.-S. Ruan, Z.-Y. Hu, D.-M. Lou, and H. Li, "Particle number emissions from a light-duty diesel engine with biodiesel fuels under transient-state operating conditions," *Applied Energy*, vol. 113, pp. 22–31, 2014.

[9] L. Chen, Z. Liang, X. Zhang, and S. Shuai, "Characterizing particulate matter emissions from GDI and PFI vehicles under transient and cold start conditions," *Fuel*, vol. 189, pp. 131–140, 2017.

[10] S. H. Lee, J. H. Kwak, S. Y. Lee, and J. H. Lee, "On-road chasing and laboratory measurements of exhaust particle emissions of diesel vehicles equipped with aftertreatment technologies (DPF, urea-SCR)," *International Journal of Automotive Technology*, vol. 16, no. 4, pp. 551–559, 2015.

[11] A. Mamakos, G. Martini, and U. Manfredi, "Assessment of the legislated particle number measurement procedure for a Euro 5 and a Euro 6 compliant diesel passenger cars under regulated and unregulated conditions," *Journal of Aerosol Science*, vol. 55, pp. 31–47, 2013.

[12] M. Masoudi, A. G. Konstandopoulos, M. S. Nikitidis et al., "Validation of a model and development of a simulator for predicting the pressure drop of diesel particulate filters," SAE Technical Paper 2001-01-0911, 2001.

[13] S. Bensaid, D. L. Marchisio, N. Russo, and D. Fino, "Experimental investigation of soot deposition in diesel particulate filters," *Catalysis Today*, vol. 147, pp. S295–S300, 2009.

[14] A. Liati and P. Dimopoulos Eggenschwiler, "Characterization of particulate matter deposited in diesel particulate filters: visual and analytical approach in macro-, micro- and nano-scales," *Combustion and Flame*, vol. 157, no. 9, pp. 1658–1670, 2010.

[15] S. Choi, K.-C. Oh, and C.-B. Lee, "The effects of filter porosity and flow conditions on soot deposition/oxidation and pressure drop in particulate filters," *Energy*, vol. 77, pp. 327–337, 2014.

[16] J. Yang, M. Stewart, G. Maupin, D. Herling, and A. Zelenyuk, "Single wall diesel particulate filter (DPF) filtration efficiency studies using laboratory generated particles," *Chemical Engineering Science*, vol. 64, no. 8, pp. 1625–1634, 2009.

[17] G. C. Koltsakis, A. Konstantinou, O. A. Haralampous, and Z. C. Samaras, "Measurement and intra-layer modeling of soot density and permeability in wall-flow filters," SAE Technical Paper 2006-01-0261, 2006.

[18] A. G. Konstandopoulos, M. Kostoglou, S. Lorentzou, and N. Vlachos, "Aspects of multifunctional diesel particulate filters and their efficient simulation," *Catalysis Today*, vol. 188, no. 1, pp. 2–13, 2012.

[19] Y. Mizuno, Y. Miyairi, F. Katsube et al., "Study on wall pore structure for next generation diesel particulate filter," SAE Technical Paper 2008-01-0618, 2008.

[20] H. Iwata, A. Konstandopoulos, K. Nakamura, T. Kasuga, K. Ogyu, and K. Ohno, "Durability of filtration layers integrated into diesel particulate filters," *SAE Technical Papers*, vol. 2, 12 pages, 2013.

[21] A. Sappok, I. Govani, C. Kamp, Y. Wang, and V. Wong, "In-situ optical analysis of ash formation and transport in diesel particulate filters during active and passive DPF regeneration processes," SAE Technical Paper 2013-01-0519, 2013.

[22] T. Bollerhoff, I. Markomanolakis, and G. Koltsakis, "Filtration and regeneration modeling for particulate filters with inhomogeneous wall structure," *Catalysis Today*, vol. 188, no. 1, pp. 24–31, 2012.

[23] M. Yu, D. Luss, and V. Balakotaiah, "Regeneration modes and peak temperatures in a diesel particulate filter," *Chemical Engineering Journal*, vol. 232, pp. 541–554, 2013.

[24] S. Bensaid, D. L. Marchisio, and D. Fino, "Numerical simulation of soot filtration and combustion within diesel particulate filters," *Chemical Engineering Science*, vol. 65, no. 1, pp. 357–363, 2010.

[25] S.-J. Lee, S.-J. Jeong, and W.-S. Kim, "Numerical design of the diesel particulate filter for optimum thermal performances during regeneration," *Applied Energy*, vol. 86, no. 7-8, pp. 1124–1135, 2009.

[26] E. Jiaqiang, W. Zuo, J. Gao, Q. Peng, Z. Zhang, and P. M. Hieu, "Effect analysis on pressure drop of the continuous regeneration-diesel particulate filter based on NO_2 assisted regeneration," *Applied Thermal Engineering*, vol. 100, pp. 356–366, 2016.

[27] A. S. Shende, J. H. Johnson, S. L. Yang, S. T. Bagley, and A. M. Thalagavara, "The filtration and particulate matter oxidation characteristics of a catalyzed wall-flow diesel particulate filter experimental and 1-D 2-layer model results," SAE Technical Paper 2005-01-0949, 2005.

[28] C. T. Huynh, J. H. Johnson, S. L. Yang, S. T. Bagley, and J. R. Warner, "A one-dimensional computational model for studying the filtration and regeneration characteristics of a catalyzed wall-flow diesel particulate filter," SAE Technical Paper 2003-01-0841, 2003.

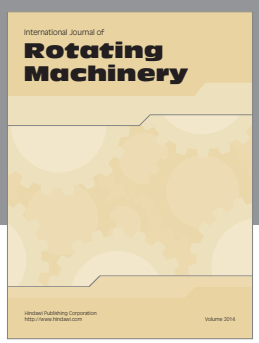

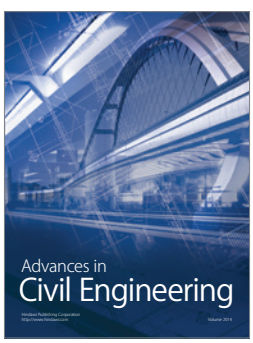

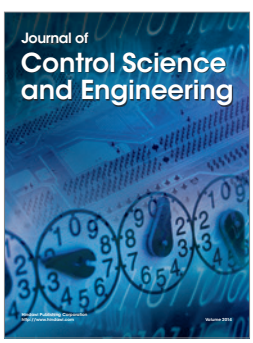

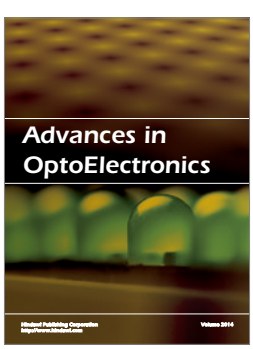

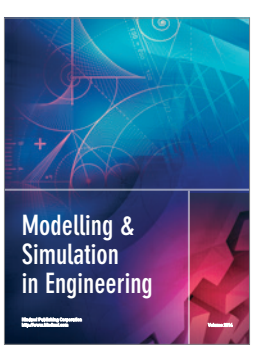

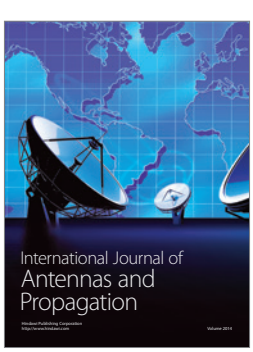

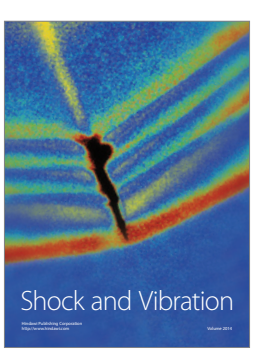

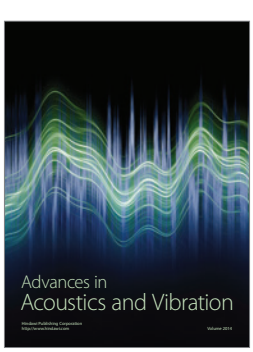

Hindawi

Submit your manuscripts at
http://www.hindawi.com